



HAL
open science

Lamins regulate nuclear mechanics and shape to control glioblastoma cell proliferation, migration and invasion

Xiuyu Wang, David Pereira, Isabelle Perfettini, Florent Peglion, Ryszard Wimmers, Ananya Roy, Karin Forsberg-Nilsson, Alexandre Baffet, Sandrine Etienne-Manneville, Jean-Baptiste Manneville

► To cite this version:

Xiuyu Wang, David Pereira, Isabelle Perfettini, Florent Peglion, Ryszard Wimmers, et al.. Lamins regulate nuclear mechanics and shape to control glioblastoma cell proliferation, migration and invasion. 2024. hal-04801952

HAL Id: hal-04801952

<https://hal.science/hal-04801952v1>

Preprint submitted on 25 Nov 2024

HAL is a multi-disciplinary open access archive for the deposit and dissemination of scientific research documents, whether they are published or not. The documents may come from teaching and research institutions in France or abroad, or from public or private research centers.

L'archive ouverte pluridisciplinaire **HAL**, est destinée au dépôt et à la diffusion de documents scientifiques de niveau recherche, publiés ou non, émanant des établissements d'enseignement et de recherche français ou étrangers, des laboratoires publics ou privés.



Distributed under a Creative Commons Attribution - NonCommercial - NoDerivatives 4.0 International License

Lamins regulate nuclear mechanics and shape to control glioblastoma cell proliferation, migration and invasion

Xiuyu Wang^{1,*}, David Pereira¹, Isabelle Perfettini², Florent Pégliion², Ryszard Wimmers³, Ananya Roy^{4,5}, Karin Forsberg-Nilsson^{4,5}, Alexandre Baffet³, Sandrine Etienne-Manneville², Jean-Baptiste Manneville^{1,*}

1 Laboratoire Matières et Systèmes Complexes, Université Paris Cité, CNRS UMR7057, 10 Rue Alice Domon et Léonie Duquet, F-75013, Paris, France

2 Cell Polarity, Migration and Cancer Unit, Institut Pasteur, CNRS, UMR3691, F-75015, Paris, France

3 Institut Curie, PSL Research University, CNRS UMR144, Paris, F-75246 France

4 Department of Immunology, Genetics and Pathology, Science for Life Laboratory, Uppsala University, Uppsala, Sweden

5 Science for Life Laboratory, Uppsala University, Uppsala, Sweden

*** Corresponding author: Jean-Baptiste.Manneville@u-paris.fr, xiuyu.wang.fr@gmail.com**

Abstract

Glioblastoma (GBM) is known as the most aggressive brain tumor and is characterized by a high heterogeneity and a median patient survival time around 15 months. Phenotyping based on cell mechanics is increasingly recognized as a potential prognostic marker for tumor aggressiveness. We have previously shown that cell and nuclear mechanical properties vary between different grades of gliomas and may be used to differentiate between GBM of different aggressiveness. Here, we find that the levels of lamin proteins can serve as an indicator of GBM aggressiveness. In patient-derived GBM cell lines, we found that cells from different GBM express different lamin levels. Nuclear size correlates positively with the ratio between lamin A and lamin B1 while nuclear stiffness increases with the levels of both lamin A and lamin B1. A simple mechanical model suggests that lamin A and lamin B1 act like springs in series. We also show that cells proliferate faster in GBM cell lines expressing higher lamin A levels. Downregulating lamin A expression in these cells reverse the aggressive phenotype. In contrast with breast cancer cells for which reduced lamin A levels favor cell migration in a confined environment, increased levels of lamin A may facilitate the invasion of more aggressive GBM cell lines in the soft environment of the brain. Furthermore, since nuclear deformation is a hallmark of malignancy in cancer cells, our results suggest that nuclear shape and mechanics may serve as prognosis biomarkers for GBM.

1 Introduction

2 Glioblastoma multiforme (GBM), recognized as the most malignant primary brain tumor with an
3 extremely poor prognosis[1], has long relied on the Tumor-Node-Metastasis (TNM) staging classification
4 as the primary parameter to gauge its degree of malignancy[2]. Despite its widespread use, the TNM
5 staging system, with GBM typically categorized as stage IV, fails to capture the considerable individual
6 variability among patients, resulting in disparate prognoses even among seemingly similar tumors[3].
7 Grade IV GBM is rare, with an age-adjusted incidence ranging from 4.67 to 5.73 cases per 100,000
8 individuals worldwide, but devastating, as there is no curative treatment available[4, 5]. Even for
9 diagnosis, only a few biomarkers are routinely used in clinical practice[6]. From diagnosis, prognosis,
10 and treatment, GBM represent a longstanding challenge for clinicians[7]. Although their precise origin
11 is still debated, GBM are thought to originate from glial cells, glial precursors or neural stem cells [8,
12 9]. In the case of isocitrate dehydrogenase (IDH)-wildtype GBMs, ventricular and outer radial glial
13 cells in the subventricular zone of the brain have been suggested to give rise to GBM cells[9].

14 Following developments in the field of mechanotransduction, more and more research emphasizes
15 that mechanical properties of both cancer cells and their environment are critical during tumour
16 development[10] and metastasis[11, 12]. Mechanosensing and mechanosignalling are altered in cancer
17 cells, which induces a remodeling of the surrounding extracellular matrix (ECM) and changes in
18 cell mechanics, in particular at the level of the nucleus. As a consequence, abnormal cell nuclear
19 morphology has often been used as a hallmark of cancer[13, 14]. In the case of glioma brain tumours,
20 nuclear shape has been used for tumour grading by histology for more than forty years[15]. Moreover,
21 *in vitro* studies using GBM cell lines have shown that substrate rigidity promotes GBM invasive
22 characteristics such as cell spreading, motility and migration, as well as proliferation[16, 17]. More
23 recent evidence shows that glioma stiffness is associated with increased mechanosensing and a highly
24 invasive mesenchymal phenotype[18] and leads to the enhanced therapeutic resistance of GBM cells[19]

25 The mechanical properties of the nucleus are thought to be critical during tumour cell invasion[20,
26 12]. Being the largest organelle in the cell, the nucleus contributes significantly to the cell mechanical
27 properties. Because cancer cells have to migrate through confined environments during tumour
28 progression and metastasis, a softer nucleus could allow cancer cells to deform more and invade
29 surrounding tissues more efficiently[21, 22]. The mechanical properties of the nucleus are imparted
30 by the nuclear envelope which separates the nucleus from the cytoplasm and the chromatin which is
31 packed inside the nucleus. Nuclear envelope mechanics is controlled by the nuclear lamina, a complex
32 network of lamin intermediate filaments constituted of lamins A/C and lamins B[23]. The nuclear
33 lamina is a dense fibrillar network underlying the inner nuclear membrane, composed primarily of A-
34 and B-type lamins, which form a two-layered structure [24]. Lamins provide mechanical support to
35 the nucleus and play a crucial role in regulating nuclear shape, stiffness, and chromatin organization
36 [25, 26, 27]. It is now becoming clear that structural proteins of the nuclear lamina not only maintain
37 a well-defined nuclear architecture but also participate in a wide range of cellular processes. For
38 instance, mutations in lamin nuclear proteins cause the so-called laminopathies[28] and dysregulation
39 of their expression is typically associated with the onset and spread of cancer[29]. The levels of lamins
40 A/C and B have also been associated with cell and tissue stiffness. An elevated ratio between the
41 expression levels of lamin A/C and the expression level of lamin B has been associated with cell and
42 tissue stiffness[30], while a decrease in lamin A/C levels facilitates migration of breast cancer cells
43 through narrow pores *in vitro*[31].

44 Here, we demonstrate that the nuclear lamin proteins play a critical role in the pathophysiology of
45 GBM. In contrast with other techniques which infer rather than directly measure nuclear mechanics,
46 we use indentation of the nucleus in living patient-derived GBM cells by internalized microspheres

47 trapped in optical tweezers to quantify the mechanical properties of the nucleus. We correlate nuclear
48 mechanics, lamin levels and indicators of GBM aggressiveness and suggest that, in contrast to what was
49 previously reported in other cancer types, GBM invasion is facilitated by increased nuclear stiffness.

50 **Materials and Methods**

51 **Cell culture.** Glioblastoma (GBM) patient-derived cells lines (U3008, U3009, U3013, U3017, U3021,
52 U3031, U3039, U3047, U3065, U3088, and U3123) were acquired from The Human Glioblastoma Cell
53 Culture Resource (HGCC, Uppsala University, Sweden, www.hgcc.se) [32], which has the necessary
54 ethical agreements to collect GBM samples from informed patients. GBM cells were cultured in
55 DMEM/F-12 (Gibco) and Neurobasal Medium (Gibco) in a 1:1 ratio, supplemented with B27 (1X,
56 Gibco), Penicillin (1%), and Epidermal growth factor (EGF, 10 ng/ml) and Fibroblast growth factor
57 (FGF, 10 ng/ml). EGF and FGF were added just before use of the culture medium. Cells were
58 cultured on Matrigel-coated plate (Gibco, Geltrex, LDEV-Free) at a concentration of 33 $\mu\text{g}/\text{ml}$. Cell
59 culture medium was changed every 3 days. Cells were passaged when 90% confluency was reached.
60 The passage ratio was between 1/10 and 1/3 depending of the cell line proliferation rate.

61 Human fetal tissue samples were collected with previous patient consent and in strict observance of
62 legal and institutional ethical regulations. The protocol was approved by the French biomedical agency
63 (Agence de la Biomédecine, approval number: PFS17-003). The dissociation and culture procedure is
64 described in [33]. Human radial glial (RG) cells were cultured in DMEM/F-12, supplemented with
65 Glucose (Sigma, 2.9mg/mL), Penicillin(1%), and Amphotericin B (250 ng/mL). B27(-vitamin A) (1X,
66 Gibco), and growth factors EGF (20 ng/ml) and FGF (20 ng/ml) were added before use. Culture
67 dishes were coated with poly-D-lysine (PDL) at 2 $\mu\text{g}/\text{cm}^2$ in Phosphate Buffered Saline (PBS) for 1
68 hour then with fibronectin at 1 $\mu\text{g}/\text{cm}^2$ for 1 hour.

69 **siRNA transfection.** Lamin A (LMNA gene) downregulation was performed using siRNA duplexes
70 specific for human LMNA (si-LaminA) purchased from Eurofins Genetics. The si-LaminA Sequence
71 (5'→3') was AGA AGG AGC UGG AGA AGA C. Luciferase was used as control. The si-Luciferase
72 Sequence (5'→3') was UAA GGC UAU GAA GAG AGA C. GBM cells were transfected at confluency
73 with si-LaminA and si-Luciferase using Lipofectamine 3000 (Thermo Fisher). Experiments were
74 performed 72 hours after transfection.

75 **Western Blotting.** Cells were lysed in RIPA buffer (Thermo Fisher) supplemented with Protease
76 inhibitor (Sigma) on ice for 10 minutes, then collected and centrifuged at maximum speed 15200
77 rpm at 4 °C for 10 minutes. Protein concentration was determined using the Bradford assay (Bio-
78 Rad Laboratories). Equal amounts of protein were mixed with reducing NuPAGE loading buffer
79 (Invitrogen), boiled and electrophoresed on NuPAGE gels (Invitrogen), and then transferred to the
80 membrane using iBlot 3 Transfer Stacks (Invitrogen). Blocking was performed for 1 hour with 5%
81 nonfat dry milk in TBST and blotting was performed with primary antibodies overnight at 4 °C.
82 Antibodies included LMNA (Abcam, SAB4200236), LMNB (Abcam, ab16048), β -actin (Proteintech,
83 66009). Quantification was carried out using ImageJ by comparing the intensity of each marker band
84 in a rectangular selection with a fixed size to that of the corresponding reference protein, β -actin in
85 the same lane.

86 **Intracellular optical-tweezers based microrheology.** Cells were plated on MatTek glass-bottom
87 dishes coated with matrigel. 2 μm -diameter fluorescent beads (Invitrogen) were added to the cell

88 culture medium at a 1:5000 dilution and were incubated with the cells for 60 hours at 37°C with 5%
89 CO₂. About 1 to 5 beads were internalized depending on the GBM cell line. Cells were stained with
90 Hoechst (33384) at a 1:10000 dilution in cell culture medium for 15 mins before the nuclear rheology
91 experiment.

92 The setup coupling optical tweezers and fast confocal microscopy has been described in detail
93 previously [34]. In brief, a single fixed optical trap was created by connecting a 1060-1100 nm infrared
94 laser beam (2 W maximum output power; IPG Photonics) to the back port of an inverted Eclipse
95 microscope (Nikon) equipped with a resonant laser confocal A1R scanner (Nikon), a 37 °C incubator,
96 and a nanometric piezostage (Mad City Labs).

97 The protocol for nuclear indentation experiments and the method for analysis was described in
98 [35]. Briefly, to indent the nucleus, a bead that initially contacted the nucleus was first trapped with
99 the laser. The piezostage was then moved at a constant speed (2.5 μm in 1 min) in order to push
100 the nucleus towards the bead. The force was deduced from the displacement of the bead from the
101 trap center (trap stiffness 240 pN/μm) and the indentation depth was obtained by image analysis. A
102 visco-elastic model was used to deduce the nuclear elasticity from the force-indentation curves [35].

103 **Immunofluorescence and confocal imaging.** GBM and RG cells were seeded on matrigel-coated
104 coverslips (33 μg/ml) overnight. Cells were fixed in 4% paraformaldehyde (Thermo Fisher) in PBS,
105 then permeabilized with 0.1% Triton-X100 for 10 min and blocked with 3% BSA-PBS (Sigma) for 1h.
106 Primary antibodies were diluted in 3% BSA-PBS and incubated for 2 hours at room temperature.
107 Secondary antibodies were diluted 1:400 in 3% BSA-PBS and incubated for 1 hour at room temperature.
108 Antibodies used are listed in the Supplementary Methods (Table S1).

109 Confocal microscopy was performed on a Zeiss LSM780 laser-scanning confocal microscope equipped
110 with white a light laser (WLL), a 405 nm diode laser, three Internal Spectral Detector Channels
111 (PMT), and two Internal Spectral Detector Channels (HyD) GaAsP. Sequential confocal images were
112 acquired using a 20x water-immersion objective (Plan-Apochromat 20x/1.0). For each staining, the
113 acquisition settings (i.e., laser power, beamsplitters, filter settings, pinhole diameters, and scan mode)
114 were kept the same. ImageJ was used to process images (see Supplementary Methods for the definition
115 of the shape parameters extracted by ImageJ).

116 **2D in vitro proliferation and migration assay and image analysis.** Cells were plated on 6-well
117 plates coated with matrigel at an initial concentration of 4000 cells/cm². The lens-free holographic
118 device Cytonote 6W (Iprasense, Helioparc, France) was used to quantify cell proliferation and to track
119 2D cell migration. Image acquisition was started 2 hours after cell seeding. Images were recorded
120 every 20 min for 72 hours. The device allows a large recording field of view (29.4 mm²). Images
121 were opened as stacks in Fiji and cells were detected automatically using the Trackmate plugin([36]).
122 Three .csv files("Spots", "Edges" and "Tracks") were extracted for each experiment. More details on
123 the extraction of migration parameters are given in Supplementary Methods (Table S2) . A custom
124 Matlab code was used to finalize graph visualization and statistical analysis.

125 **In vivo invasion assay.** *In vivo* analysis of GBM cells invading the zebrafish brain was performed
126 as previously described [37, 38]. In brief, zebrafish larvae of Tg(fli1a:rfp) to mark endogenous blood
127 vessels were obtained from fertilized zebrafish eggs 3 days prior to xenotransplantation. Larvae were
128 made transparent by preventing melanin pigmentation using N-phenylthiourea (PTU) (0.003% final).
129 Larvae of 3 dpf were mounted in 2.5 mm wide V-shaped agarose trenches and microinjected after
130 160 mg/L tricaine treatment using a mechanical micromanipulator (CellTram oil vario microinjector,

131 5176000.025, Eppendorf) with GBM cells expressing GFP. 2.5 % of a an 80 % confluent 10 cm Petri
132 dish of GBM cells in 5 μ l PBS was microinjected into the zebrafish Optic Tectum just above the
133 Middle Cerebral Vein at a maximum of 100 μ m from the surface. Xenografts containing a single
134 tumor mass formed by 20-50 cells located in the top 200 μ m from the Optic Tectum were selected.
135 After 4 hours of recovery at 32 °C, the larvae were mounted for imaging in a 1% low-melting agarose
136 solution in a 35 mm diameter glass-bottom video-imaging dish. A Nikon Ti2E spinning-disk confocal
137 microscope was used to image the tumor cell mass and invaded cells at 4h and 72h post-injection. The
138 Imaris software was used to segment the cells and calculate the 3D area occupied by the tumor cell
139 mass and invaded cells. The invasion index was calculated as the ratio between the averaged distance
140 travelled by the top 10 cells at 72 hours compared to 4 hours.

141 **Statistical analysis.** All data are presented as mean values \pm standard error mean (s.e.m.) of at
142 least three ($N \geq 3$) independent experiments. In nuclear rheology experiments, at least $n > 30$ nucleus
143 were measured in each condition. Violin plots show the median value (dashed line), and the first and
144 third quartiles (dotted lines). Error bars correspond to s.e.m. Statistical relevance was evaluated using
145 Student's t-test or one-way ANOVA test with GraphPad Prism, depending on the number of cells,
146 number of samples, and the normality of the distribution. For protein expression levels measured from
147 Western Blot experiments, a one-way ANOVA test was used to compare the protein levels in each
148 GBM cell line to RG cells. For protein downregulation by siRNA, a t-test was used to compare to the
149 siLuciferase control. p-values are reported as non-significant (n.s. $p > 0.05$, p-values are indicated), or
150 significant * $p < 0.05$, ** $p < 0.01$, *** $p < 0.001$, **** $p < 0.0001$).

151 Correlation analysis was performed using Spearman's rank correlation analysis. Curve-fitting was
152 done using either linear fits or nonlinear fits including one-phase decay with or without plateau.
153 Correlation and curve fitting were performed with GraphPad Prism.

154 Results

155 Patient-derived glioblastoma cell lines upregulate lamin A

156 We have previously shown that a grade IV GBM cell line exhibits elevated expression of lamin A
157 and a stiffer nucleus compared to a grade III counterpart [35]. This observation prompted us to study
158 the potential influence of nuclear mechanics on GBM aggressiveness, with a focus on the role of lamin
159 proteins. We selected eleven patient-derived GBM cell lines. These include four proneural subtype
160 cell lines: U3008, U3013, U3021, and U3047; four classical subtype cell lines: U3009, U3017, U3039,
161 and U3123; and three mesenchymal subtype cell lines: U3031, U3065, and U3088. As a non-tumoural
162 control, we used radial glial (RG) cells.

163 We found that lamin protein expression exhibits distinct patterns between the patient-derived
164 GBM cell lines and RG cells. Specifically, lamin A expression levels are higher in all GBM cell lines,
165 whereas RG cells show very low expression (Fig. 1a-b). Nine out of the eleven cell lines demonstrate a
166 significantly higher lamin A expression level compared to RG cells (Fig. 1c). The expression pattern
167 of lamin C closely mirrors that of lamin A (Fig. 1d, Supplementary Fig. S1a, Supplementary Table
168 S3). However, since RG cells display higher expression of lamin C than lamin A, lamin A appears to
169 be a more suitable biomarker to distinguish GBM cells from RG cells.

170 The expression of lamin B1 exhibited more variability and did not correlate with lamin A expression
171 (Supplementary Fig. S1b). Some GBM cell lines exhibited increased expression of lamin B1 compared
172 to RG cells, while others showed decreased expression levels (Fig. 1e). Together these results show

173 that, among the three lamin proteins studied, lamin A emerges as the key discriminator between
174 GBM and RG cells.

175 **A- and B-type lamins have opposing effects on nuclear morphology.**

176 By visualizing the nucleus and lamin proteins, we found that nuclear morphology is very het-
177 erogeneous between GBM cell lines and between GBM and RG cells (Fig. 1a). We categorized
178 nuclear shapes into two groups: regular and irregular which encompassed features such as elongated,
179 donut-shape, curved and blebbing nuclei (Supplementary Fig. S1c-d). In GBM cells, we observed
180 that at least 40% of the nuclei display irregular shapes, with some cell lines exhibiting a majority
181 (60–70%) of irregular nuclei (Fig. 1f). Conversely, in RG cells, less than 3% of nuclei are found to be
182 irregular. In addition to exhibiting abnormal shapes, maximum projections of confocal images unveiled
183 significant alterations in nuclear size. Overall, GBM cells display larger nuclear areas compared to
184 RG cells. For instance, the average nucleus projected area of U3008 cells is approximately $300 \mu\text{m}^2$,
185 four times larger than the nuclear size of RG cells.

186 We then asked whether lamin levels could play a role in the nuclear morphology of GBM cells.
187 We found a weak positive correlation between nuclear size and the expression levels of lamin A and
188 lamin C and a weak negative correlation between nuclear size and the expression levels of lamin B
189 (Supplementary Fig. S2). Interestingly, the size of the nucleus strongly correlates with the ratio
190 between lamin A and lamin B1 (Fig. 1g-h). Nonlinear regression analyses (one-phase decay) revealed
191 a significant correlation between the nuclear projected area or perimeter and the ratio between lamin
192 A and lamin B1 expression levels (termed A/B1 ratio in the following) across the eleven GBM cell
193 lines and RG cells (Fig. 1g,h, Supplementary Tables S4, S5), indicating that the influence of lamin
194 expression on cell nuclear size is not restricted to a specific cell line. We did not observe similar
195 correlations among GBM cells between the expression levels of lamin proteins and the proportion of
196 irregular nuclei (Supplementary Fig. S3) or nuclear morphological parameters, such as circularity,
197 roundness, and shape index (Supplementary Fig. S4). Both increases in nuclear-projected area and
198 perimeter as a function of the A/B1 ratio are well described by an exponential saturation with a
199 plateau value at high (> 20) A/B1 ratios:

$$f(R_{A/B1}) = (Y_{min} - Y_{max}) * e^{-k*(R_{A/B1})} + Y_{max} \quad (1)$$

200 where $R_{A/B1}$ is the A/B1 ratio, and Y_{min} and Y_{max} are the minimal and maximum nuclear-projected
201 area or perimeter, respectively. Curve fitting gives $Y_{min} = 97.59\mu\text{m}^2$, $Y_{max} = 311.4\mu\text{m}^2$, $k = 0.1588$
202 for the nuclear projected area and $Y_{min} = 45.14\mu\text{m}$, $Y_{max} = 82.09\mu\text{m}$, $k = 0.1293$ for the nuclear
203 projected perimeter.

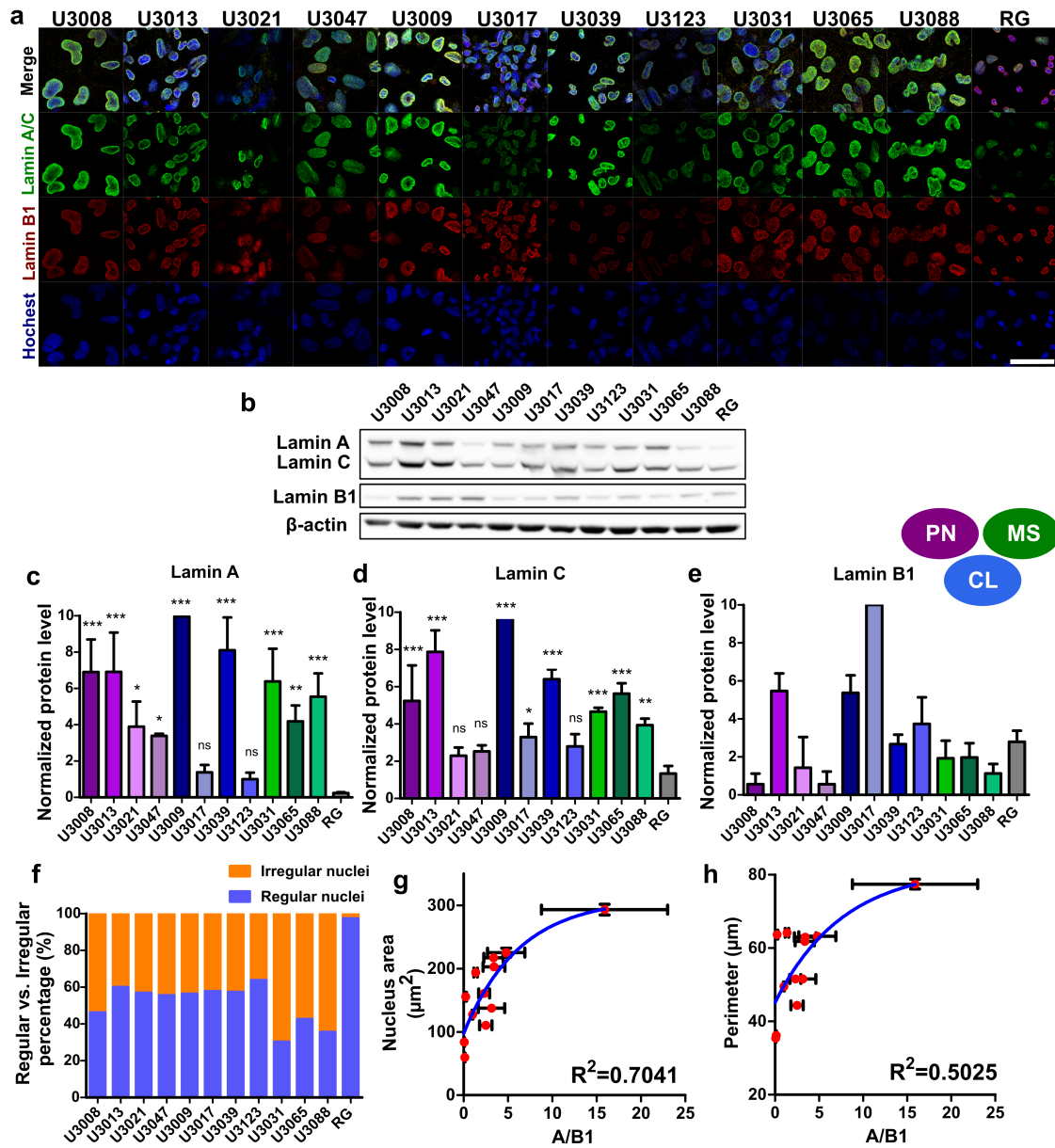


Figure 1: **A- and B-type lamins are differently expressed in GBM cells and have opposing effects on nuclear morphology in GBM cells.** **a** Immunostaining images of GBM cell lines and RG cells. Lamin A/C (green), Lamin B1 (red). DNA was counterstained with Hoechst (blue). Scale bar 50 μm . **b** Western blot of lamin A/C and lamin B1. β -actin was used as a loading control. **c-e** Densitometric analyses for lamin A, lamin C, and lamin B1 respectively. The graphs are shown as mean values \pm SEM of three different experiments. Asterisks indicate statistically significant differences with respect to control RG cells; one-way ANOVA test, n.s. $p > 0.05$, * $p < 0.05$, ** $p < 0.01$, *** $p < 0.001$. Colors indicate the GBM subtype (purple, proneural PN; blue, classical CL; green, mesenchymal MS). **f** Proportions of nuclei displaying regular vs. irregular shapes in GBM cells and RG cells. At least 100 nuclei were analyzed for each cell line. **g** Correlation between the nuclear area and the lamin ratio A/B1. The fitting curve follows a one-phase decay. Spearman test $R^2=0.8322$, $p=0.0008$ (***). **h** Correlation between the nuclear perimeter and the lamin ratio A/B1. The fitting curve follows a one-phase decay. Spearman test $R=0.5874$, $p=0.0446$ (*).

204 Lamin A and Lamin B1 increase nuclear elasticity collaboratively.

205 Because GBM cells and RG cells exhibit variable lamin levels which correlate with changes in
206 nuclear morphology, we next asked whether nuclear mechanics also differ in these cell populations. To
207 address this issue, we used optical tweezers (OT) microrheology [34, 35] to quantify the elasticity of
208 the nucleus. Nuclear indentation experiments (Supplementary Movies S1-S2) allowed us to distinguish
209 between 'soft' and 'stiff' nuclei (Fig. 2a,b). Notably, softer nuclei exhibited heightened susceptibility to
210 deformation, resulting in an extended retention time of laser-held beads during nuclear movement
211 ($2.5\mu\text{m}/60\text{s}$). Conversely, stiffer nuclei exhibited reduced compliance, causing early escape of the bead
212 from the laser trap. Consequently, for soft nuclei, we observed pronounced nucleus deformations
213 coupled with small bead displacements from the optical trap center, corresponding to low forces, while
214 stiff nuclei displayed reduced nucleus deformations and large bead displacements from the optical trap
215 center corresponding to large forces (Fig. 2a,b). The nucleus elasticity was measured by fitting the
216 force-indentation curves with a visco-elastic model [35].

217 Our results show that the elasticity of the nucleus varies significantly between distinct cell lines.
218 Specifically, within the cohort of patient-derived GBM cell lines, a comparison between the regular
219 and irregular nuclei subgroups unveiled inherent differences in nucleus elasticity. In the regular nuclei
220 group, GBM cell lines consistently exhibit larger nucleus elasticity than RG cells. The difference
221 is particularly pronounced in U3013, U3009, and U3039 cell lines, for which significant differences
222 with RG cells are observed (Fig. 2c). In the irregular nuclei group, nuclear stiffness is more variable
223 within a given cell line (Fig. 2d), probably because of the local nature of the measurement. This
224 observation underscores the complex interplay between nuclear architecture and cellular heterogeneity
225 in the context of GBM. Remarkably, we found that the elasticity of irregular nuclei is generally lower
226 than that of regular nuclei within the same cell line (Fig. 2e). However, two exceptions were noted in
227 cell lines with low lamin levels, U3017 and U3047.

228 We found that nuclear elasticity weakly correlates with the levels of lamin A, lamin B1 and lamin
229 C, and the ratio A/B1 (Supplementary Fig. S5a-c), while it correlates with the sum of the expression
230 levels of lamin A and lamin B1 denoted as $A + B1$ (Supplementary Fig. S5d, Supplementary Tables
231 S6, S7). Interestingly, we found that nuclear elasticity correlates much more strongly with a lamin
232 level L defined by $1/L = 1/A + 1/B1$ or $L = (A * B1)/(A + B1)$, where A is the expression level
233 of lamin A and $B1$ is the expression level of lamin B1. Assuming that the two 'layers' of Lamin
234 A and Lamin B1 act mechanically as springs in series, L represents the effective lamin level which

235 may participate in nuclear mechanics. Consistently, when plotted as a function of the effective lamin
236 level L , we found that the nuclear elasticity K measured by OT for both regular and irregular nuclei
237 increases with L (Fig. 2f-g, Supplementary Tables S8, S9) and is well adjusted by a one-phase decay
238 non-linear regression corresponding to:

$$K(L) = \begin{cases} K_{min}, & (L < L_0) \\ K_{max} + (K_{min} - K_{max}) * e^{-a*(L-L_0)}, & (L > L_0) \end{cases} \quad (2)$$

- 239 – K_{min} denotes the minimum elasticity of the nucleus at low L values.
- 240 – L_0 is the critical effective lamin level above which nuclear elasticity is sensitive to L .
- 241 – a denotes the cell sensitivity to the effective lamin level L , representing the rate at which nuclear
242 elasticity increases with L .
- 243 – K_{max} is the maximum elasticity achievable by the nucleus at high lamin levels. Once the nucleus
244 reaches this value, further increase in lamin levels does not result in significant increase in
245 elasticity.

246 For regular nuclei, the fit parameters are $L_0 = 0.48$, $a = 0.95$, $K_{min} = 141.4$, and $K_{max} = 316.5$ and
247 nuclear elasticity ranges from 140 to 307 $pN/\mu m$, from U3047 to U3009 GBM cell lines, respectively.
248 The effective lamin level L exhibits a range of 0.2 to 3.5, from RG cells to the U3009 GBM cell line.

249 For irregular nuclei, the fit parameters are $L_0 = 0.84$, $a = 1.69$, $K_{min} = 144.1$, and $K_{max} = 274.1$ and
250 nuclear elasticity ranges from 119 to 287 $pN/\mu m$, from U3021 to U3039 GBM cell lines, respectively.
251 The effective lamin level L exhibits a range of 0.5 to 3.5, from U3008 to U3009 GBM cell lines,
252 respectively.

253 Regarding the minimum stiffness of the nucleus K_{min} , our analysis indicates a similar basal elasticity
254 for both regular and irregular nuclei. Regarding L_0 , in the regular group, nuclear elasticity initiates its
255 increase when the effective lamin level reaches 0.48. In contrast, within the irregular group, the effective
256 lamin level needs to reach 0.84 before influencing nuclear stiffness. Regarding a , interestingly, nuclear
257 elasticity increases faster with L in the irregular group compared to the regular group. Regarding K_{max} ,
258 we found that the plateau value of irregular nuclei is 10% smaller than that of regular nuclei, suggesting
259 a lower maximum elasticity threshold in irregular nuclei compared to their regular counterparts.

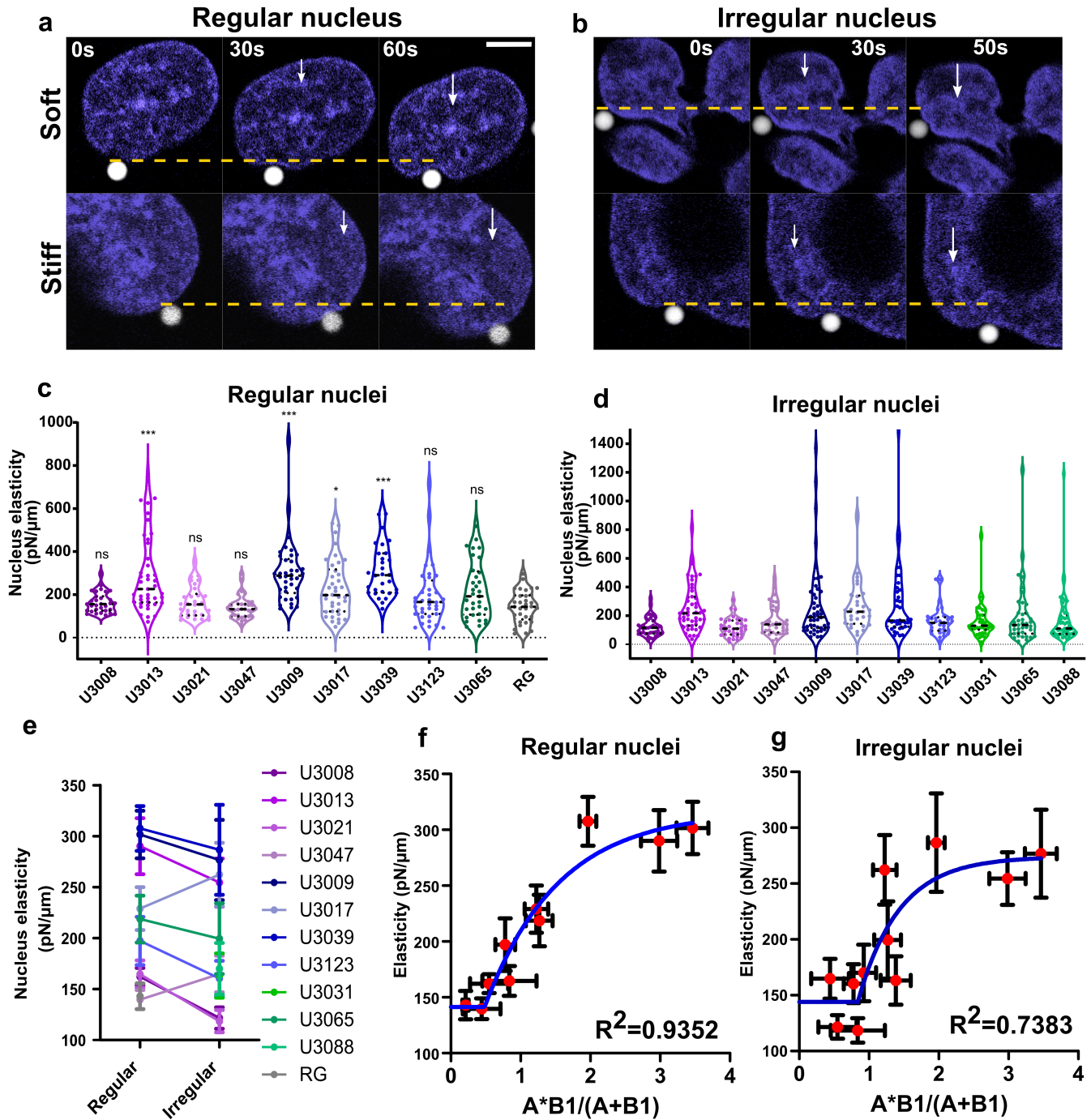


Figure 2: **Differences in nuclear elasticity between GBM cell lines correlate with lamin levels.** **a,b** Time-lapse images of regular (a) and irregular (b) nucleus indentation. The white arrow indicates the direction in which the nucleus is moved. The dotted line marks the initial position of the fluorescent bead in the center of the trap. Bead diameter: $2\ \mu\text{m}$. Scale bar $5\ \mu\text{m}$. **c** Violin plot of OT measurements of the elasticity of regular nuclei in 9 GBM cell lines and in RG cells ($N \geq 3$, $n \geq 30$ cells). U3031 and U3088 cells did not have a sufficient number of regular nuclei for measurement. **d** Violin plot of OT measurements of the elasticity of irregular nuclei in 11 GBM cell lines ($N \geq 3$, $n \geq 30$ cells). RG cells did not have a sufficient number of irregular nuclei for measurement. **e** Comparison of the OT measurement of nuclear elasticity for regular and irregular nuclei in each cell line. **f** Correlation between the elasticity of regular nuclei and the lamin ratio $(A \cdot B1)/(A+B1)$. The fitting curve follows a one-phase decay with an initial plateau. Spearman test $R^2=0.9273$, $p=0.001$ (***) . **g** Correlation between the elasticity of irregular nuclei and the lamin ratio $(A \cdot B1)/(A+B1)$. The fitting curve follows a one-phase decay with an initial plateau. Spearman test $R^2=0.7273$, $p=0.0112$ (*).

260 GBM cell proliferation correlates positively with Lamin A expression levels.

261 Our results so far show that lamin expression levels in patient-derived GBM cell lines are associated
262 with nuclear morphology and elasticity. In contrast with other cancer types for which tumour
263 progression is characterized by cell and nucleus softening [12, 29], we have previously reported that a
264 grade IV GBM cell line exhibits a stiffer nucleus than a grade III glioma cell line [35]. Hence, we aimed
265 here to investigate in more detail the impact of lamin A on GBM aggressiveness in patient-derived
266 cell lines.

267 We first measured cell proliferation rates, as an indicator of aggressiveness, using lens-free microscopy
268 in the eleven patient-derived GBM cell lines and in RG cells (Supplementary Movie S3) and found
269 very different proliferation profiles (Fig. 3a-b). For instance, U3088 cells, U3008 cells, and RG cells
270 show high, medium, and low proliferation rates, respectively. Cell lines with low proliferation rates
271 exhibit a 1.5-2 fold increase in cell number in 72 hours, while cell lines with high proliferation rates
272 reach up to a 3-5 fold increase in cell number (Fig. 3b). Notably, RGs cells proliferate the slowest
273 among the twelve cell lines we studied.

274 We then asked whether lamin expression levels correlate with the proliferation rate (Figure 3c,
275 Supplementary Fig. S6a). Plotting the proliferation rate against the lamin A expression level revealed
276 a statistically significant positive correlation (Supplementary Table S10): cell lines with higher lamin
277 A expression consistently exhibit higher proliferation rates, while those with low lamin A expression
278 display lower proliferation rates. Figure 3c illustrates that RG cells and the four GBM cell lines with
279 low lamin A expression (below 4 a.u.) exhibit less than a 2-fold increase in cell number in 72 hours,
280 while the remaining seven cell lines, with lamin expression ranging from 4 a.u. to 10 a.u., exhibit a 2
281 to 5-fold increase in cell number. A similar correlation was observed with lamin C expression levels
282 (Supplementary Table S11) but not with lamin B1 expression levels (Supplementary Fig. S6a) or with
283 the combinations of lamin levels (Supplementary Fig. S6c)

284 Given our results showing a link between lamin levels and nuclear morphology and mechanics (Figs.
285 1 and 2, Supplementary Figures S1-S5), we expected that nuclear morphological and mechanical
286 characteristics could impact on cell proliferation. We indeed found that the proportion of irregular
287 nuclei positively correlates with the rate of cell proliferation, as depicted in Figure 3d, although not in a
288 statistically significant manner (Supplementary Table S12). Similarly and not surprisingly since nuclear
289 elasticity and lamin A expression levels strongly correlates (Supplementary Fig. S5a-b), proliferation
290 rates positively correlate with the elasticity of regular nuclei (Figure 3e, Supplementary Table S13)

291 and, although to a lesser extent, of irregular nuclei (Supplementary Fig. S6b, Supplementary Table
292 S14).

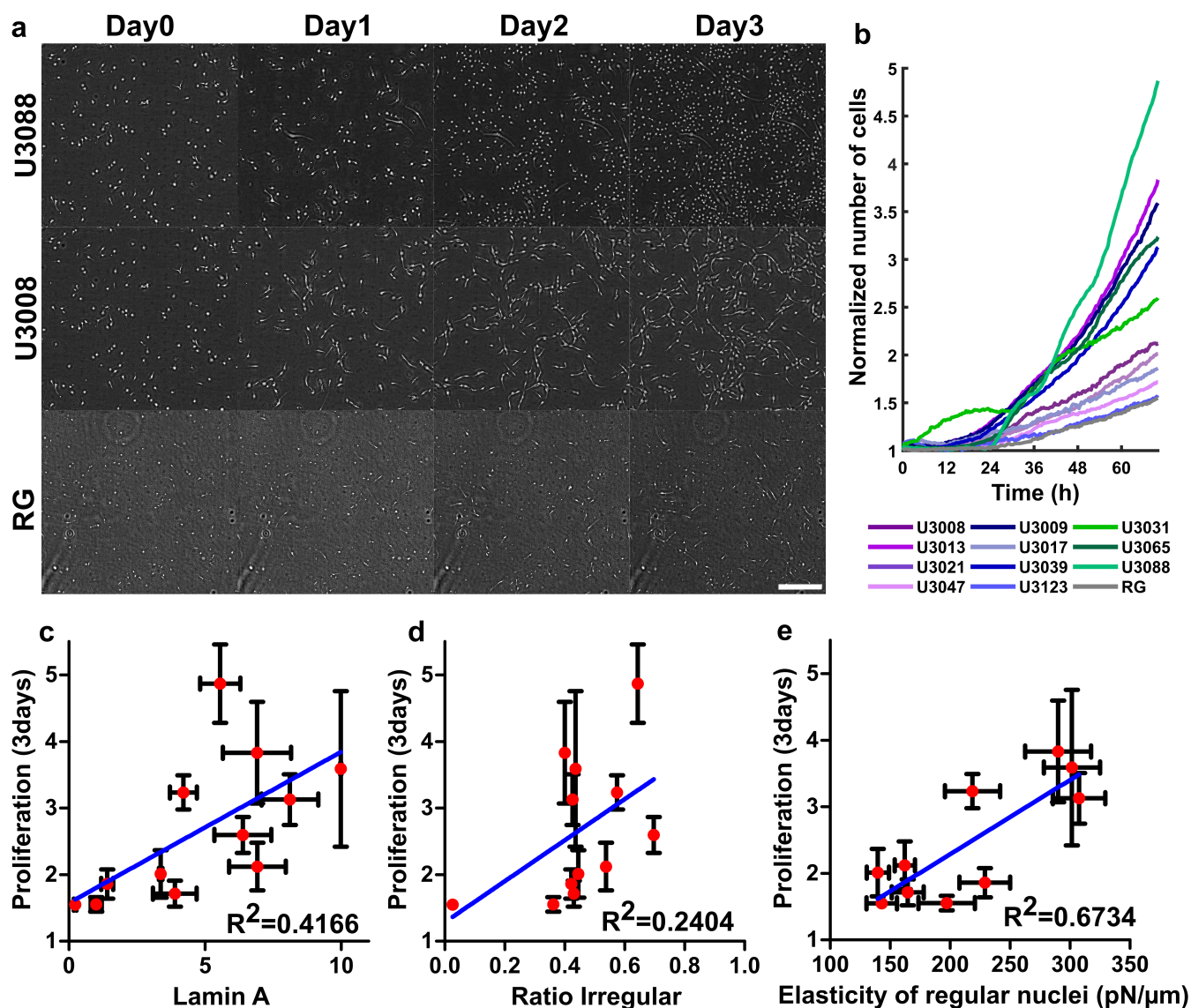


Figure 3: GBM cell lines expressing high levels of lamin A show elevated proliferation rates. **a** Brightfield lens-free microscopy images of 2D cell cultures followed for three days. U3088, U3008, and RG cells represent high, medium, and low proliferation rates, respectively. Scale bar 500 μ m. **b** Time evolution of cell proliferation on a 2D substrate during three days. (N=3 independent experiments, $n \geq 2000$ cells). For a better readability of the figure, error bars are not shown but can be appreciated from panels c-e. **c** Correlation between proliferation and lamin A levels. **d** Correlation between proliferation and the proportion of irregular nuclei. **e** Correlation between proliferation and nucleus elasticity.

293 **2D migration velocity of GBM cells correlates positively with Lamin A** 294 **expression levels.**

295 GBM clinically display diverse motile and invasive capacities. Here, we first used migration on 2D
296 substrates as a second indicator for the aggressiveness of our patient-derived GBM cell lines. The 2D
297 migration of single cells was tracked for three days for the eleven GBM cell lines and for RG cells
298 using lens-free microscopy. RG cells are the slowest moving cells with an average speed of $0.3 \mu\text{m}/\text{min}$
299 and GBM cell lines migrate much faster and exhibit a range of migration velocities (Fig 4a). 2D
300 migration velocity increases with increasing lamin expression levels (Fig 4b, Supplementary Fig. S7a).
301 With the exception of two GBM cell lines of the classical subtype with low lamin A expression levels,
302 2D migration velocity strongly correlates with lamin A expression levels (Fig 4b). We found that
303 2D cell migration velocity weakly correlates with the expression levels of lamin B1 and lamin C or
304 the combinations of lamin levels (Supplementary Fig. S7a-b). Interestingly, we found that the 2D
305 migration velocity correlates linearly with nuclear elasticity (Fig. 4c, Supplementary Tables S15, S16).

306 *In vivo*, the proliferation rate and migration velocity are two important indicators of the degree of
307 malignancy of a tumour, as they determine the growth rate and metastatic potential of a tumour.
308 These two indicators are not necessarily related. Indeed, when the data of the three GBM subtypes
309 were pooled, we did not observe any clear correlation between proliferation rate and 2D migration
310 velocity (Supplementary Fig. S7c). However, once grouped by subtype, 2D cell migration velocity
311 and proliferation rate positively correlate for cell lines of the proneural and classical subtypes, while
312 they were negatively correlated for cell lines of the mesenchymal subtype (Supplementary Fig. S7c).
313 Interestingly, cells of the classical subtype move twice as fast as those of the proneural subtype
314 (Supplementary Fig. S7c).

315 **Impact of lamin A on glioblastoma invasion**

316 Our results show that lamin A levels are associated with both GBM cell proliferation and 2D
317 migration (Figs. 3 and 4a-c). However, proliferation and migration on a 2D stiff substrate is not always
318 indicative of the invasion rate in three-dimensional tissues. We thus asked whether lamin A expression
319 levels could affect the invasiveness of GBM cells. To address this question, we injected cancer cells
320 into the brain of zebrafish and compares the invasion of five different GBM cell lines. These cell lines
321 (U3013, U3039, U3065, U3088, and U3123) were selected for their diversity in their expression levels
322 of lamin A, the mechanical and morphological properties of their nucleus, and their behaviours in
323 the 2D cell proliferation and migration assays. We found that these five GBM cell lines had a very
324 different invasion rate (Fig.4 d) as quantified using their invasion index (see Methods). Unexpectedly,
325 the U3123 cell line, which expressed the lowest amount of lamin A, did not invade the zebrafish brain
326 and died 24 hours after injection (Fig. 4e, d). Furthermore, we observed a positive correlation between
327 the lamin A expression levels and the invasion index for the remaining four cell lines (Fig. 4f). The
328 U3039 cell line, which expresses the highest level of lamin A, had the highest invasion index which was
329 statistically significantly higher than for the U3065 and U3088 cell lines (Fig.4 d, e). Taken together
330 our results demonstrate that, in GBM, the lamin A expression level impacts on nuclear morphology
331 and mechanical properties and positively correlates with cell proliferation and migration in 2D and
332 with cell invasion in the zebrafish brain, which can be considered as indicators of GBM aggressiveness.

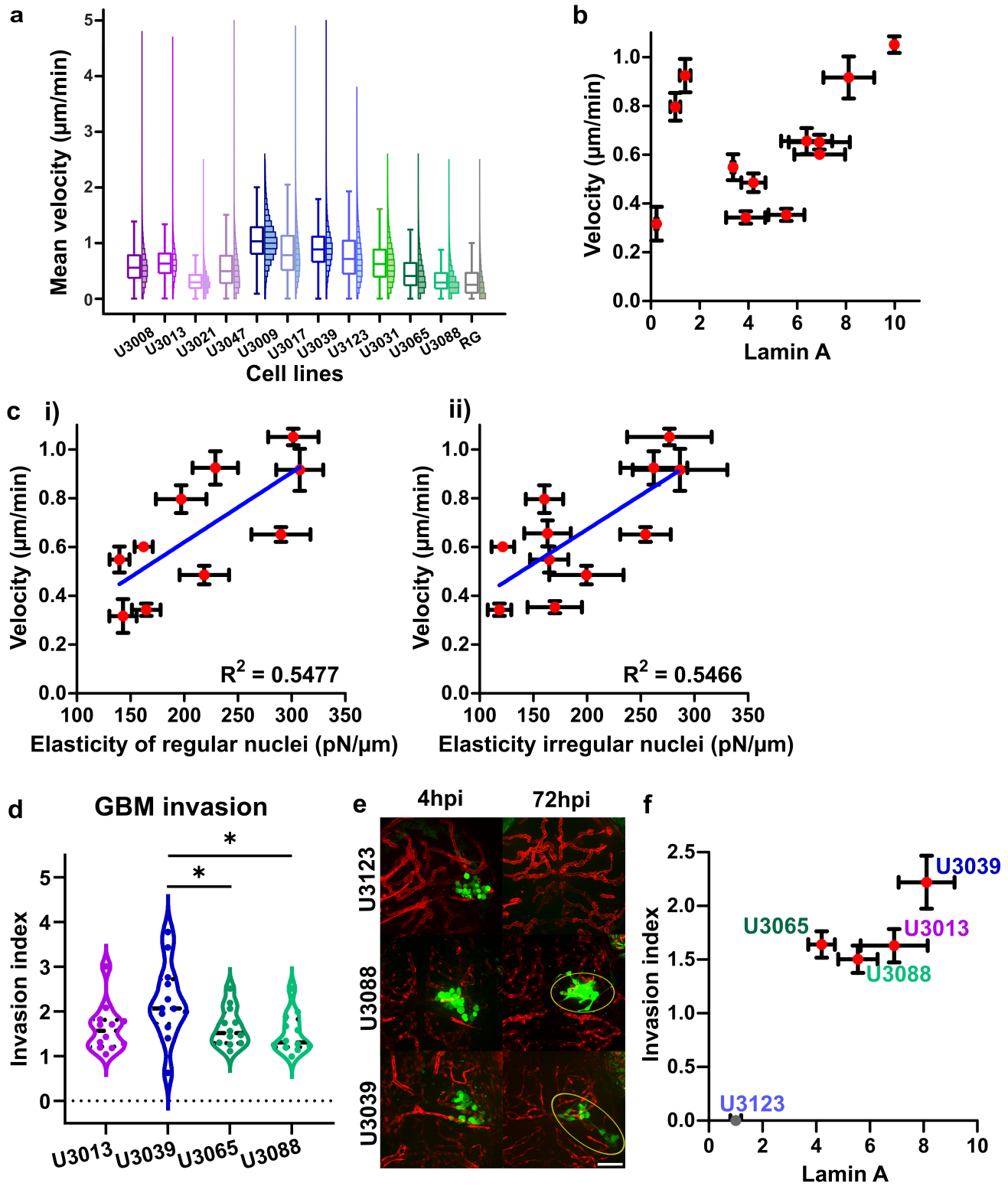


Figure 4: **GBM cell lines expressing high levels of lamin A show elevated 2D migration velocity and higher invasion in the zebrafish brain.** **a** Histo-box plot of cell migration velocity. The results show the mean velocity along the track of single cells during 3 days (N=3 independent experiments, $n \geq 2000$ cells). **b** Correlation between migration velocity and lamin A level. **c** Correlation between cell velocity and nuclear elasticity for regular nuclei (i) and for irregular nuclei (ii). **d** Violin plot of the invasion index of four GBM cell lines (U3013, U3039, U3065, U3088) in the zebrafish brain. **e** Fluorescence images of GBM cell lines (U3123, U3088, U3039) invasion in the zebrafish brain (GBM cells in green, endothelial cells delineating blood vessels in red) at 4 hours and 72 hours post-injection (hpi) (N=8 zebrafish larvae, $n \geq 10$ cells). Yellow circles in the 72hpi U3088 and U3039 images indicate the zone of invasion. U3123 cells do not survive in the zebrafish brain. Scale bar, 50 μm . **f** Correlation between the expression level of lamin A and the invasion index in the zebrafish brain of the four GBM cell lines shown in d). Note that we added the U3123 data with a zero invasion index, as this cell line does not survive in the zebrafish brain.

333 **Downregulating lamin A expression reduces nuclear size, nuclear elasticity,** 334 **proliferation and 2D migration velocity in GBM cells**

335 To further test the potential causal links between lamin levels and GBM aggressiveness, we studied
336 the effects of lamin A downregulation on nuclear morphology and mechanics and on cell proliferation
337 and migration. We used siRNA-mediated downregulation of lamin A (si-Lamin A) in two GBM cell
338 lines, U3009 and U3039 which are both of the classical subtype and have the highest lamin A expression
339 levels among our eleven GBM cell lines. As a control, siRNA against Luciferase (si-Luciferase) was
340 used. We checked the effect of lamin A downregulation by immunostaining and Western blot (Fig. 5a,
341 b). Quantification of the Western blot results show that the lamin A expression levels was decreased
342 by 30-40% compared to the control group in both cell lines three days after siRNA transfection (Fig.
343 5c).

344 We first investigated the effects of lamin A downregulation on nuclear morphology and found
345 that both U3009 and U3039 cells treated with si-Lamin A have smaller nuclei than control cells
346 (Supplementary Fig. S8). In the case of U3039 cells, the nucleus projected area is reduced by
347 30% after lamin A downregulation. In the case of U3009 cells, lamin A downregulation does not
348 induce any change in the nucleus projected area but decreases the nucleus thickness by around 30%
349 (Supplementary Fig. S8).

350 We next asked whether the mechanical properties of the nucleus are affected by lamin A downregulation.
351 We observed a 30% decrease in nuclear elasticity following lamin downregulation (Fig. 5d),
352 showing that lamin A contributes to nuclear elasticity and explaining the correlation between lamin A
353 levels and nuclear elasticity (Supplementary Fig. S5).

354 We also measured the impact of lamin A downregulation on two indicators of GBM aggressiveness,
355 2D cell proliferation and migration velocity. We found a strong decrease in the proliferation rate of
356 both U3009 and U3009 cells treated with si-Lamin A compared with the control (Fig. 5e). Note
357 that, even with a modest (30%) decrease in lamin A expression (Fig. 5a-c), the proliferation rate is
358 decreased to the same level as RG cells, our control cells. Similarly, we measured a significant decrease
359 in 2D migration velocity after lamin A downregulation (Fig. 5f). These results demonstrate that
360 decreasing lamin A expression levels can efficiently reduce GBM cell proliferation and migration in 2D.

361 Finally, to test the potential clinical relevance of our results, we correlated the lamin A expression
362 levels of the primary cell lines with the survival time of the corresponding patients. Although the
363 survival time strongly depends on the age at which the patient is first diagnosed with GBM, the

364 survival of patients with low lamin A levels (U3123, U3017, U3047, U3021, U3065) was higher than
365 that of patients with high lamin A levels (U3088, U3031, U3013, U3008, U3039, U3009) within the first
366 year after diagnosis (Fig. 5g panel i), although not in a statistically significant manner. Consistently,
367 the patient survival time appears to decrease with the lamin A expression level in ten out of the eleven
368 patient-derived GBM cell lines (Fig. 5g panel ii), with the notable exception of the outlier U3039 cell
369 line. These observations suggest that lamin A expression may be used as a prognosis marker for GBM.

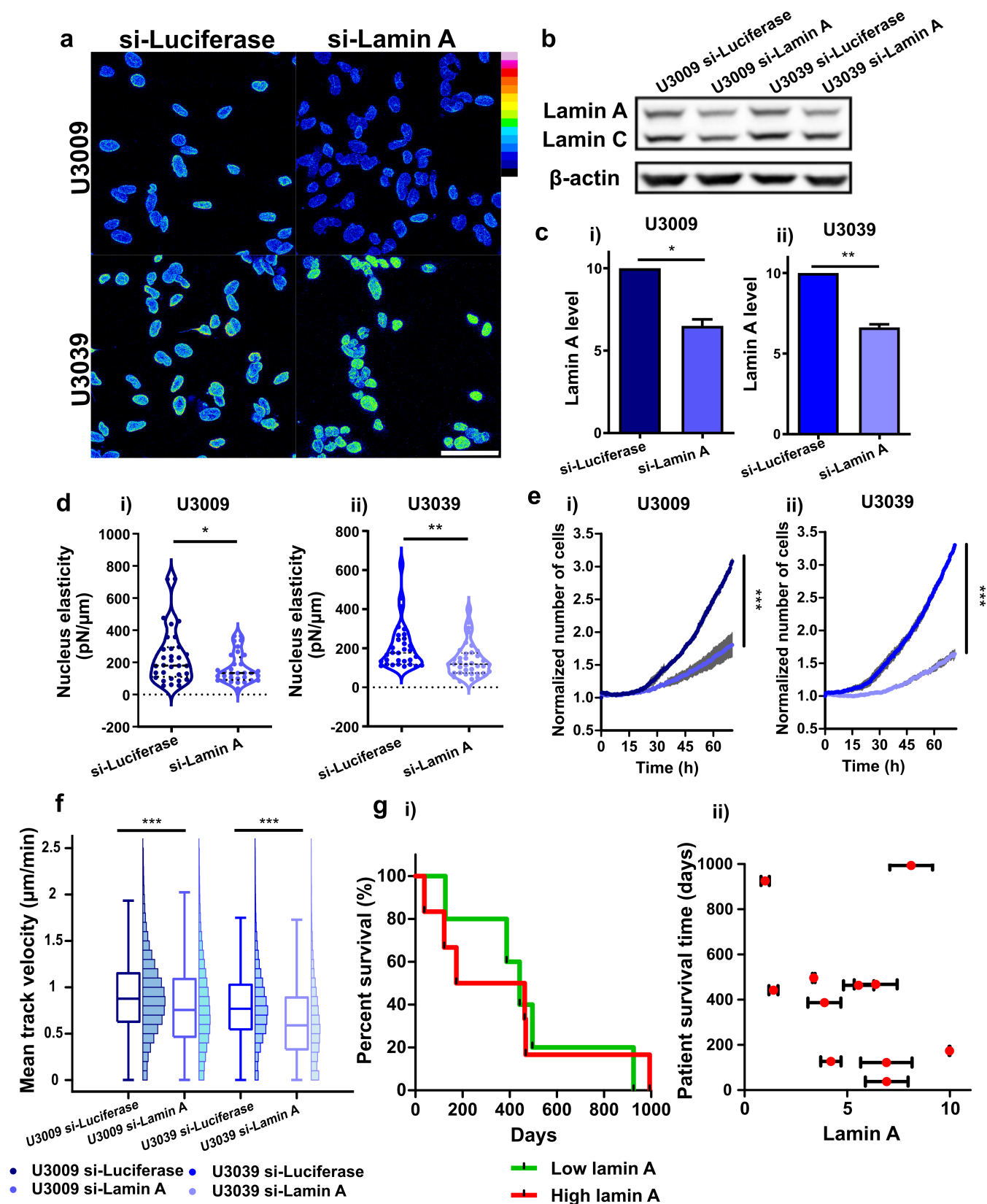


Figure 5: **Downregulation of lamin A induces a decrease in nuclear elasticity, proliferation and 2D migration.** **a** Immunostaining images of U3009 and U3039 cells treated with si-Lamin A and si-Luciferase as a control. Scale bar, 50 μm . **b** Western blot showing the reduction of lamin A expression in si-Lamin A treated cells compared to control si-Luciferase treated cells. β -actin was used as a loading control. **c** Quantification of lamin A levels from the Western blot results. Both U3009 (i) and U3039 (ii) cells treated with si-Lamin A show a 30-40% decrease in lamin A expression compared to control cells. **d** Violin plots of nuclear elasticity measured by intracellular OT for U3009 (i) and U3039 (ii) cells treated with si-Lamin A or control si-Luciferase ($N \geq 3$, $n \geq 30$ cells). **e** Time evolution of cell proliferation on 2D substrates during three days for U3009 (i) and U3039 (ii) cells treated with si-Lamin A or control si-Luciferase ($N = 3$, $n \geq 2000$ cells). **f** Histo-box plot of cell migration velocity for U3009 and U3039 cells treated with si-Lamin A or control si-Luciferase. The results show the mean velocity along the track of single cells during three days ($N = 3$, $n \geq 2000$ cells). **g** Clinical data of patient survival. i) Kaplan-Meier plot of patient survival percentage for GBM patients expressing high levels of lamin A (U3088, U3031, U3013, U3008, U3039, U3009) or low levels of lamin A (U3123, U3017, U3047, U3021, U3065). ii) Correlation between patient survival time (in days) and lamin A expression levels. In panels (a-f), the graphs show mean values \pm SEM of three different experiments. Asterisks indicate statistically significant differences between si-Lamin A and si-Luciferase treated U3009 or U3039 cells; t-test, n.s. $p > 0.05$, * $p < 0.05$, ** $p < 0.01$, *** $p < 0.001$.

370 Discussion

371 The mechanical properties of the cell and in particular those of its nucleus are thought to be critical
372 for cancer cell migration and invasion. While tumour progression has been associated with cell and
373 nuclear softening in several types of cancers, we have previously shown that, for glioma tumours, a
374 grade IV GBM cell line exhibits a stiffer cytoplasm and nucleus than a grade III cell line [35]. These
375 results lead us to hypothesize that nuclear stiffening may be associated to glioma aggressiveness. Here
376 we test this hypothesis in the context of GBM using eleven patient-derived cell lines and non tumoral
377 RG cells. We find that the regulation of nuclear morphology and stiffness by lamins is associated with
378 GBM cell proliferation, migration, and invasion.

379 Lamins and nuclear morphology in GBM cells.

380 Lamin proteins are known to regulate nuclear shape in several cell types. For instance, lamin B
381 deletion has been shown to induce nuclear blebbing [39] in HeLa cells. It was also observed that lamin
382 B1 stabilizes the nucleus shape by restricting outward protrusions of the lamin A/C network [40].
383 High-resolution imaging has shown that nuclear blebs localize at zones lacking lamin B [40], suggesting
384 distinct roles of lamin A/C and lamin B in nuclear morphology. Lamin A is supposed to expand the
385 nucleus, whereas lamin B contracts it [40, 41]. Previous studies have demonstrated the opposing roles
386 of lamin A and lamin B in determining cell nuclear morphology [42]. Here we confirm these results in
387 GBM cells. We show that the ratio between the expression levels of lamin A and lamin B1 (A/B1
388 ratio) positively correlates with nuclear size (Fig. 1g,h, Supplementary Fig. S2) and that reducing
389 lamin A expression levels by about 30-40% decreases nuclear size in two GBM cell lines with high
390 lamin A expression levels (Supplementary Fig. S8). We also distinguished between cells exhibiting a
391 'regular' and an 'irregular' nucleus (Supplementary Fig. S1c,d) and found that all GBM cells have a
392 much higher proportion of irregular nuclei than RG cells (Fig. 1f) but no correlation was observed
393 with the expression levels of lamin proteins (Supplementary Fig. S3).

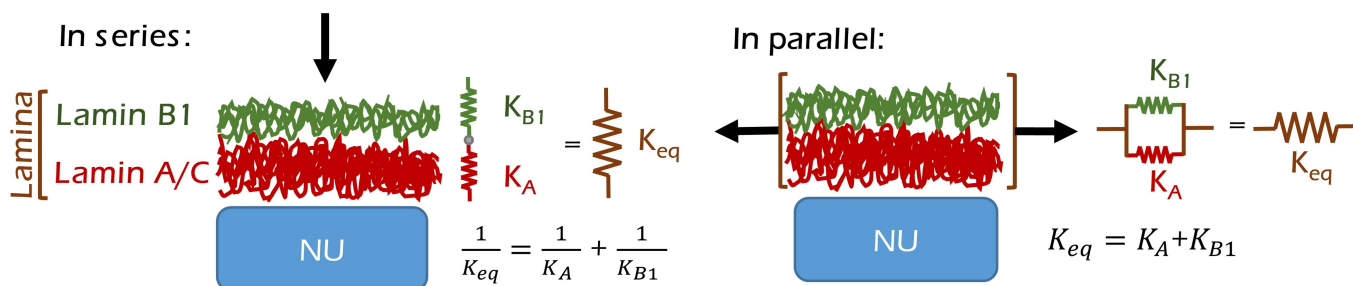


Figure 6: **Mechanical models of the nuclear lamina.** The two layers of lamin A and lamin B1 can act mechanically as springs in series (left panel) or in parallel (right panel).

394 Lamins and the mechanical properties of the nucleus in GBM cells.

395 The role of lamins in the control of nuclear mechanics is well established, in particular in the case
 396 of lamin A [43, 44]. In agreement with previous results, downregulating lamin A expression by siRNA
 397 in two GBM cell lines expressing high levels of lamin A (U3009 and U3039) reduces nucleus elasticity
 398 (Fig. 5d). The contribution of lamin B1 to the stiffness of the nucleus is more controversial but lamin
 399 B1 does seem to significantly affect the mechanical properties of the nucleus[45]. Tissue and cell
 400 stiffness have been shown to correlate primarily with lamin A expression levels [30]. Furthermore, it
 401 was recently shown that the loss of A- or B- type lamins significantly softens the nucleus [42].

402 Here we show that, the mechanical properties of the nucleus (Fig. 2) depend on both lamin A and
 403 lamin B1, suggesting a physical link between the two networks of intermediate filament proteins.
 404 Although the lamin A and lamin B1 networks are known to localize in close proximity at the nuclear
 405 lamina [40], no direct interaction between lamin A and lamin B1 has been reported so far [27, 46].
 406 From a mechanical point of view, depending on their spatial arrangement, the two lamin networks
 407 can act as mechanical viscoelastic modules in series or in parallel. Considering only the elasticity of
 408 the two networks, the equivalent elasticity K is given by $K = K_A + K_{B1}$ if lamin A and lamin B1 act
 409 in parallel and by $K = K_A * K_{B1} / (K_A + K_{B1})$, where K_A is the elasticity of the lamin A network and
 410 K_{B1} is the elasticity of the lamin B1 network (Fig.6).

411 When studying the mechanics of our different GBM cell lines and RG cells, we found that nuclear
 412 elasticity increases with the quantity L defined by $L = A * B1 / (A + B1)$ where A is the expression
 413 level of lamin A and $B1$ is the expression level of lamin B1 (Fig.2f,g). Nuclear elasticity correlates
 414 more strongly with the quantity L than with individual lamin levels (A , C or $B1$), with the $A/B1$
 415 ratio or with the $A + B1$ sum which would correspond to a model in which the lamin networks act
 416 in parallel (Supplementary Fig. S5). Our data thus strongly favors a physical model in which the
 417 lamin A and lamin B1 networks act as springs in series. This finding is supported by the localization
 418 of the two networks as two superimposed layers when imaged with super-resolution microscopy [40],
 419 with the lamin B1 localizing more externally than the lamin A network in the nuclear lamina. Such a
 420 two-layer spatial arrangement of the two networks is consistent with the idea that B-type lamins tend
 421 to contract the nucleus while A-type lamins tend to increase nuclear size [40, 41] as discussed above.
 422 The two-layer model of the lamin A and lamin B1 networks may also explain the mechanical coupling
 423 between the two networks: by compressing the nucleus, an increase in lamin B1 levels in the outer
 424 lamina could induce an increase in lamin A concentration in the internal lamina and a subsequent
 425 increase in nuclear stiffness. Note that the precise relative localization of the lamin B1 and lamin A
 426 networks is still debated and the two networks may actually be intertwined.

427 Together our measurements of nuclear elasticity with optical tweezers in living cells point to a

428 synergy between the lamin A and lamin B1 networks in the control of nuclear mechanics. To better
429 understand this synergy, we used a one-phase decay non-linear regression to fit the evolution of the
430 nuclear elasticity $K(L)$ as a function of the effective lamin level L (Equation 2). For both regular
431 and irregular nuclei, we found that above a threshold value L_0 , the nuclear elasticity increases from a
432 minimum value K_{min} to a maximum plateau value K_{max} with a sensitivity a to the effective lamin level
433 L . As discussed below, the values of these four parameters (L_0 , K_{min} , K_{max} , and a) differ between
434 regular and irregular nuclei.

435 At low lamin levels, below the L_0 threshold, the elasticity of the nucleus is small ($K \simeq K_{min}$) and
436 does not vary significantly with L . This observation suggests that our optical tweezers techniques
437 probes mostly the mechanics of a lamin-independent component of the nucleus, probably intra-nuclear
438 material such as chromatin. The value of the minimal elasticity K_{min} is not only similar for RG
439 cells and GBM expressing low lamin levels but also for both regular and irregular nuclei in these cell
440 lines (Fig. 2f,g and Supplementary Tables S8, S9), strengthening our hypothesis that lamins do not
441 contribute to nuclear elasticity below an effective lamin level threshold L_0 . Above the L_0 threshold,
442 the nuclear elasticity increases with the effective lamin level L , confirming the known impact of lamins
443 on nuclear mechanics [43, 44, 42]. At high lamin expression levels ($L \gg L_0$, the nuclear elasticity
444 saturates. Interestingly, irregular nuclei exhibit a sharper increase in elasticity with a higher threshold
445 value L_0 and a higher sensitivity a and reach a lower K_{max} value (about 10% lower) than regular
446 nuclei. It has been reported that the lamin B1 network is disorganized or even lacking from regions of
447 local nuclear deformations [40, 47] such as in blebbing, elongated, protruding or donut shapes typical
448 of irregular nuclei (Supplementary Fig. S1c-d). Because our optical tweezers technique probes nuclear
449 mechanics locally, the lower average elasticity we measured for irregular nuclei for most GBM cell
450 lines (Fig. 2c-e) could thus result from heterogeneities in the distribution of the lamin B1 network.

451 Lamins and GBM cell proliferation, migration and invasion.

452 Our results not only confirm and specify the role of lamin proteins in the control of nuclear shape
453 and mechanical properties but also highlight their links with other cellular functions in GBM cells. In
454 particular, we demonstrate that the expression level of lamin A correlates with GBM cell proliferation
455 (Fig. 3) and that downregulating lamin A reduces cell proliferation (Fig.5e). Both A-type lamins and
456 B-type lamins have been linked with cell proliferation in previous studies [48, 49, 24]. Silencing lamin
457 A/C in human fibroblasts [48] or knocking-out lamin A in mouse [49] reduces cell proliferation, in
458 agreement with our results. Lamins are known to anchor chromatin at the nuclear envelope and to
459 influence higher-order chromatin organization due to their capacity to bind DNA, chromosomes, and
460 chromatin[50]. Lamins may play a role in the cell cycle-dependent dynamics of nuclear structure since
461 they reversibly separate from chromosomes during mitosis in a phosphorylation-dependent manner [51].
462 Although the precise mechanisms by which lamin A may promote GBM cell proliferation have to be
463 investigated in more details, our data show a clear link between lamin levels and GBM aggressiveness
464 through cell proliferation.

465 Another hallmark of GBM cells is their extremely high migratory and invasive capacities [52]. In
466 particular, we have shown previously that cytoplasmic intermediate filaments, in particular vimentin
467 intermediate filaments, play a crucial role in GBM cell migration [52, 38]. Here, we find that 2D
468 migration velocity positively correlates with lamin A levels (Fig. 4b and Fig. 5f). Similarly GBM cell
469 lines which express more lamin A invade more efficiently the zebrafish brain (Fig.4d-f). Because we
470 showed that GBM cell lines with higher lamin levels display a stiffer nucleus, our data suggest that
471 in GBM, in contrast with previous results in other types of cancers such as breast cancer[53, 54], a
472 stiffer nucleus allows more efficient cell migration and invasion. These results are consistent with our

473 previous report that a less aggressive astrocytoma grade III cell line display a softer nucleus than a
474 more aggressive GBM grade IV cell line [35]. Still they may seem surprising when compared to other
475 tumours for which a softer nucleus may allow cells to be more deformable and hence migrate more
476 efficiently through entangled and confined extracellular matrices (ECM) [35, 55, 31]. Our data favor a
477 model in which a stiff nucleus allows cells to push more efficiently through the soft environment of the
478 brain [56].

479 *In vivo*, GBM cell migration occurs as chain migration along blood vessels, known as vessel co-
480 option[57]. It was recently shown that GBM cells that use vessel co-option to invade the mouse brain
481 exhibit high levels of lamin A [58]. In agreement, in our zebrafish model, we observed that higher
482 lamin A expression correlates with more efficient invasion. This suggests that during chain migration
483 along blood vessels, leader cells with a stiff nucleus, high contractility, and a high matrix degradation
484 activity [38] may 'dig' more efficiently through the brain ECM and allow follower cells to migrate in
485 their tracks. Taken together, our data suggest that GBM cells expressing higher levels of lamins show
486 a more aggressive phenotype which may be, at least in part, attributed to an increase in the stiffness
487 of the nucleus.

488 Clinical perspectives

489 In a vast majority of cancer types, including prostate cancer[59], colon cancer[60], gastrointestinal
490 neoplasms[61], gastric carcinoma[62], breast cancer[63] and neuroblastoma[64], decreased lamin A
491 levels have been associated to a higher degree of malignancy[65]. In some cases, the contribution of
492 lamin A to cancer cell invasion is more debated[66]. In contrast, we demonstrate here that lamin levels
493 positively correlate with GBM cell proliferation, migration and invasion, suggesting that up-regulation
494 of lamins, and in particular lamin A, may favor GBM aggressiveness. This specificity of GBM may be
495 explained by the low expression levels of lamins in the healthy brain as compared to other tissues. In
496 organs that are inherently subject to mechanical stress, including the breast, the prostate, the intestine
497 and the pancreas, lamin A is highly expressed in the healthy tissues [30, 29], and decreased lamin A
498 levels is a hallmark of cancer in the tumoral tissues[29]. In the brain, however, lamin A is expressed
499 at very low levels in most cell types including neurons, glial progenitor cells, and astrocytes[67,
500 68]. Depending on the role and the level of expression of lamins in the tissue of origin, tumour
501 development may thus be characterized by an down-regulation or an up-regulation of lamins. This
502 hypothesis is further supported in the case of the brain by the observation that most LMNA-negative
503 laminopathy patients do not exhibit significant abnormalities or brain developmental defects during
504 fetal development[69], but will later develop cardiac and/or skeletal myopathy. Conversely, for B-type
505 lamins which are strongly expressed in brain tissues compared to lamin A[67, 68], LMNB-negative
506 laminopathy can cause fetal death as well as major defects in the patient's brain and nervous system
507 during development[70].

508 Finally, we noticed that survival was higher for patients with low lamin A expression levels one year
509 after diagnosis, and that, with one exception out of the eleven patient-derived GBM cells we studied,
510 the patient survival time decreased with increasing lamin A expression levels (Fig. 5g). Together
511 with our *in vitro* data and our results in the zebrafish brain, this observation further suggests that
512 lamins may serve as clinically relevant therapeutic targets. To conclude, our study highlights the
513 role of lamins in GBM aggressiveness through their impact on nuclear shape and mechanics. Further
514 work should address the potential mechanisms linking the roles of lamins in cell proliferation and cell
515 invasion with their roles in nuclear mechanics, in the context not only of GBM but also of other types
516 of cancers or other diseases.

517 Acknowledgments

518 This work was supported by grants from ITMO Cancer Inserm-Aviesan "Approches interdisci-
519 plinaires des processus oncogéniques et perspectives thérapeutiques : Apports à l'oncologie de la
520 physique, de la chimie et des sciences de l'ingénieur" Edition 2022" (NUTMEG project, grant number
521 22CP073-00) and from the Labex Who Am I? (ANR-11-LABX-0071) and the "Initiatives d'excellence"
522 (Idex ANR-11-IDEX-0005-02) transverse project BioMechanOE (TP5).

523 Author contribution statements

524 [Jean-Baptiste Manneville] conceptualized the study, and supervised the overall project. [Xiuyu
525 Wang] designed and performed the experiments; collected and analyzed the data; and interpreted the
526 results. [David Pereira] performed optical tweezers experiments. [Isabelle Perfettini, Florent Peglion,
527 Sandrine Etienne-Manneville] provided the zebrafish model and performed invasion experiments in
528 zebrafish. [Ryszard Wimmers, Alexandre Baffet] collected and differentiated radial glial cells. [Ananya
529 Roy, Karin Forsberg-Nilsson] provided GBM cell lines and expertise in GBM biology. [Xiuyu Wang]
530 was responsible for writing the first draft of the manuscript. All authors contributed to the review
531 and editing of the manuscript, approved the final version, and agreed to be accountable for all aspects
532 of the work.

References

- [1] Farina Hanif et al. “Glioblastoma multiforme: a review of its epidemiology and pathogenesis through clinical presentation and treatment”. In: *Asian Pacific journal of cancer prevention: APJCP* 18.1 (2017), p. 3.
- [2] James D Brierley, Mary K Gospodarowicz, and Christian Wittekind. *TNM classification of malignant tumours*. John Wiley & Sons, 2017.
- [3] R Stupp et al. “High-grade glioma: ESMO Clinical Practice Guidelines for diagnosis, treatment and follow-up”. In: *Annals of oncology* 25 (2014), pp. iii93–iii101.
- [4] Sheila K Singh et al. “Identification of human brain tumour initiating cells”. In: *nature* 432.7015 (2004), pp. 396–401.
- [5] Chul-Kee Park, Jeong Mo Bae, and Sung-Hye Park. “Long-term survivors of glioblastoma are a unique group of patients lacking universal characteristic features”. In: *Neuro-Oncology Advances* 2.1 (2020), vdz056.
- [6] Wojciech Szopa et al. “Diagnostic and therapeutic biomarkers in glioblastoma: current status and future perspectives”. In: *BioMed research international* 2017 (2017).
- [7] Kaja Urbańska et al. “Glioblastoma multiforme—an overview”. In: *Contemporary Oncology/Współczesna Onkologia* 18.5 (2014), pp. 307–312.
- [8] Aneta Włodarczyk et al. “Gaps and doubts in search to recognize glioblastoma cellular origin and tumor initiating cells”. In: *Journal of oncology* 2020.1 (2020), p. 6783627.
- [9] Elena Verdugo, Iker Puerto, and Miguel Ángel Medina. “An update on the molecular biology of glioblastoma, with clinical implications and progress in its treatment”. In: *Cancer Communications* 42.11 (2022), pp. 1083–1111.
- [10] Valentin Gensbittel et al. “Mechanical adaptability of tumor cells in metastasis”. In: *Developmental cell* 56.2 (2021), pp. 164–179.
- [11] FuiBoon Kai, Allison P Drain, and Valerie M Weaver. “The extracellular matrix modulates the metastatic journey”. In: *Developmental cell* 49.3 (2019), pp. 332–346.
- [12] Charlotte Alibert, Bruno Goud, and Jean-Baptiste Manneville. “Are cancer cells really softer than normal cells?” In: *Biology of the Cell* 109.5 (2017), pp. 167–189.
- [13] Douglas Hanahan. “Hallmarks of cancer: new dimensions”. In: *Cancer discovery* 12.1 (2022), pp. 31–46.
- [14] Kin-Hoe Chow, Rachel E Factor, and Katharine S Ullman. “The nuclear envelope environment and its cancer connections”. In: *Nature Reviews Cancer* 12.3 (2012), pp. 196–209.
- [15] H Martin et al. “Automated image analysis of gliomas an objective and reproducible method for tumor grading”. In: *Acta neuropathologica* 63 (1984), pp. 160–169.

- [16] Katarzyna Pogoda et al. “Compression stiffening of brain and its effect on mechanosensing by glioma cells”. In: *New journal of physics* 16.7 (2014), p. 075002.
- [17] Thomas James Grundy et al. “Differential response of patient-derived primary glioblastoma cells to environmental stiffness”. In: *Scientific reports* 6.1 (2016), p. 23353.
- [18] J Matthew Barnes et al. “A tension-mediated glycocalyx–integrin feedback loop promotes mesenchymal-like glioblastoma”. In: *Nature cell biology* 20.10 (2018), pp. 1203–1214.
- [19] Ariane E Erickson et al. “Fabrication and characterization of chitosan–hyaluronic acid scaffolds with varying stiffness for glioblastoma cell culture”. In: *Advanced healthcare materials* 7.15 (2018), p. 1800295.
- [20] Celine Denais and Jan Lammerding. “Nuclear mechanics in cancer”. In: *Cancer biology and the nuclear envelope: Recent advances may elucidate past paradoxes* (2014), pp. 435–470.
- [21] Claudia Tanja Mierke. “The fundamental role of mechanical properties in the progression of cancer disease and inflammation”. In: *Reports on Progress in Physics* 77.7 (2014), p. 076602.
- [22] Claudia Tanja Mierke. “The matrix environmental and cell mechanical properties regulate cell migration and contribute to the invasive phenotype of cancer cells”. In: *Reports on Progress in Physics* 82.6 (2019), p. 064602.
- [23] Yosef Gruenbaum and Roland Foissner. “Lamins: nuclear intermediate filament proteins with fundamental functions in nuclear mechanics and genome regulation”. In: *Annual review of biochemistry* 84.1 (2015), pp. 131–164.
- [24] Youngjo Kim. “The impact of altered lamin B1 levels on nuclear lamina structure and function in aging and human diseases”. In: *Current Opinion in Cell Biology* 85 (2023), p. 102257. ISSN: 0955-0674. DOI: <https://doi.org/10.1016/j.ceb.2023.102257>. URL: <https://www.sciencedirect.com/science/article/pii/S0955067423001060>.
- [25] Robert D Goldman et al. “Nuclear lamins: building blocks of nuclear architecture”. In: *Genes & development* 16.5 (2002), pp. 533–547.
- [26] Thomas Dechat et al. “Nuclear lamins”. In: *Cold Spring Harbor perspectives in biology* 2.11 (2010), a000547.
- [27] Amnon Buxboim et al. “Scaffold, mechanics and functions of nuclear lamins”. In: *FEBS letters* 597.22 (2023), pp. 2791–2805.
- [28] Howard J Worman. “Nuclear lamins and laminopathies”. In: *The Journal of pathology* 226.2 (2012), pp. 316–325.
- [29] Niina Dubik and Sabine Mai. “Lamin A/C: function in normal and tumor cells”. In: *Cancers* 12.12 (2020), p. 3688.
- [30] Joe Swift et al. “Nuclear lamin-A scales with tissue stiffness and enhances matrix-directed differentiation”. In: *Science* 341.6149 (2013), p. 1240104.
- [31] Celine M Denais et al. “Nuclear envelope rupture and repair during cancer cell migration”. In: *Science* 352.6283 (2016), pp. 353–358.
- [32] Yuan Xie et al. “The human glioblastoma cell culture resource: validated cell models representing all molecular subtypes”. In: *EBioMedicine* 2.10 (2015), pp. 1351–1363.

- [33] Laure Coquand et al. “A cell fate decision map reveals abundant direct neurogenesis bypassing intermediate progenitors in the human developing neocortex”. In: *Nature Cell Biology* 26.5 (May 2024), pp. 698–709. ISSN: 1476-4679. DOI: [10.1038/s41556-024-01393-z](https://doi.org/10.1038/s41556-024-01393-z). URL: <https://doi.org/10.1038/s41556-024-01393-z>.
- [34] David Guet et al. “Mechanical role of actin dynamics in the rheology of the Golgi complex and in Golgi-associated trafficking events”. In: *Current Biology* 24.15 (2014), pp. 1700–1711.
- [35] Charlotte Alibert et al. “Multiscale rheology of glioma cells”. In: *Biomaterials* 275 (2021), p. 120903.
- [36] Jean-Yves Tinevez et al. “TrackMate: An open and extensible platform for single-particle tracking”. In: *Methods* 115 (2017), pp. 80–90.
- [37] Sandrine Etienne-Manneville, Florent Peglion, and Franck Coumailleau. “Live Imaging of Microtubule Dynamics in Glioblastoma Cells Invading the Zebrafish Brain”. In: *JoVE* 185 (July 2022). Publisher: MyJoVE Corp, e64093. ISSN: 1940-087X. DOI: [10.3791/64093](https://doi.org/10.3791/64093). URL: <https://app.jove.com/64093>.
- [38] Emma J van Bodegraven et al. “Intermediate filaments promote glioblastoma cell invasion by controlling cell deformability and mechanosensitive gene expression”. In: (2023). DOI: [10.21203/rs.3.rs-2828066/v1](https://doi.org/10.21203/rs.3.rs-2828066/v1).
- [39] Takeshi Shimi et al. “The A-and B-type nuclear lamin networks: microdomains involved in chromatin organization and transcription”. In: *Genes & development* 22.24 (2008), pp. 3409–3421.
- [40] Bruce Nmezi et al. “Concentric organization of A-and B-type lamins predicts their distinct roles in the spatial organization and stability of the nuclear lamina”. In: *Proceedings of the National Academy of Sciences* 116.10 (2019), pp. 4307–4315.
- [41] Takeshi Shimi et al. “Structural organization of nuclear lamins A, C, B1, and B2 revealed by superresolution microscopy”. In: *Molecular biology of the cell* 26.22 (2015), pp. 4075–4086.
- [42] Amir Vahabikashi et al. “Nuclear lamin isoforms differentially contribute to LINC complex-dependent nucleocytoplasmic coupling and whole-cell mechanics”. In: *Proceedings of the National Academy of Sciences* 119.17 (2022), e2121816119.
- [43] Jan Lammerding et al. “Lamin A/C deficiency causes defective nuclear mechanics and mechanotransduction”. In: *The Journal of clinical investigation* 113.3 (2004), pp. 370–378.
- [44] Patricia M Davidson and Jan Lammerding. “Broken nuclei–lamins, nuclear mechanics, and disease”. In: *Trends in cell biology* 24.4 (2014), pp. 247–256.
- [45] Jan Lammerding et al. “Lamins A and C but not lamin B1 regulate nuclear mechanics”. In: *Journal of Biological Chemistry* 281.35 (2006), pp. 25768–25780.
- [46] Nana Naetar, Simona Ferraioli, and Roland Foisner. “Lamins in the nuclear interior- life outside the lamina”. In: *Journal of cell science* 130.13 (2017), pp. 2087–2096.
- [47] Natalie Y Chen et al. “An absence of lamin B1 in migrating neurons causes nuclear membrane ruptures and cell death”. In: *Proceedings of the National Academy of Sciences* 116.51 (2019), pp. 25870–25879.
- [48] Olga Moiseeva et al. “Retinoblastoma-independent regulation of cell proliferation and senescence by the p53–p21 axis in lamin A/C-depleted cells”. In: *Aging Cell* 10.5 (2011), pp. 789–797. DOI: <https://doi.org/10.1111/j.1474-9726.2011.00719.x>.

- [49] T Sullivan et al. “Loss of A-type lamin expression compromises nuclear envelope integrity leading to muscular dystrophy”. en. In: *J. Cell Biol.* 147.5 (Nov. 1999), pp. 913–920.
- [50] Vicente Andrés and José M González. “Role of A-type lamins in signaling, transcription, and chromatin organization”. In: *Journal of Cell Biology* 187.7 (2009), pp. 945–957.
- [51] Josef Gotzmann and Roland Foisner. “Lamins and lamin-binding proteins in functional chromatin organization”. In: *Critical Reviews™ in Eukaryotic Gene Expression* 9.3-4 (1999).
- [52] Cécile Leduc and Sandrine Etienne-Manneville. “Intermediate filaments in cell migration and invasion: the unusual suspects”. In: *Current opinion in cell biology* 32 (2015), pp. 102–112.
- [53] Guilherme Pedreira de Freitas Nader et al. “Compromised nuclear envelope integrity drives TREX1-dependent DNA damage and tumor cell invasion”. In: *Cell* 184.20 (2021), 5230–5246.e22. ISSN: 0092-8674. DOI: <https://doi.org/10.1016/j.cell.2021.08.035>. URL: <https://www.sciencedirect.com/science/article/pii/S0092867421010461>.
- [54] Tony Fischer, Alexander Hayn, and Claudia Tanja Mierke. “Effect of Nuclear Stiffness on Cell Mechanics and Migration of Human Breast Cancer Cells”. In: *Frontiers in Cell and Developmental Biology* 8 (2020). ISSN: 2296-634X. DOI: [10.3389/fcell.2020.00393](https://doi.org/10.3389/fcell.2020.00393). URL: <https://www.frontiersin.org/journals/cell-and-developmental-biology/articles/10.3389/fcell.2020.00393>.
- [55] Takamasa Harada et al. “Nuclear lamin stiffness is a barrier to 3D migration, but softness can limit survival”. In: *Journal of Cell Biology* 204.5 (2014), pp. 669–682.
- [56] Carlos F Guimarães et al. “The stiffness of living tissues and its implications for tissue engineering”. In: *Nature Reviews Materials* 5.5 (2020), pp. 351–370.
- [57] Giorgio Seano and Rakesh K Jain. “Vessel co-option in glioblastoma: emerging insights and opportunities”. In: *Angiogenesis* 23.1 (2020), pp. 9–16.
- [58] Rajesh Kumar Gupta et al. “Tumor-specific migration routes of xenotransplanted human glioblastoma cells in mouse brain”. In: *Scientific Reports* 14.1 (2024), p. 864.
- [59] Sergej Skvortsov et al. “Proteomics profiling of microdissected low-and high-grade prostate tumors identifies Lamin A as a discriminatory biomarker”. In: *Journal of proteome research* 10.1 (2011), pp. 259–268.
- [60] EJ Th Belt et al. “Loss of lamin A/C expression in stage II and III colon cancer is associated with disease recurrence”. In: *European journal of cancer* 47.12 (2011), pp. 1837–1845.
- [61] SF Moss et al. “Decreased and aberrant nuclear lamin expression in gastrointestinal tract neoplasms”. In: *Gut* 45.5 (1999), pp. 723–729.
- [62] Zhengrong Wu et al. “Reduced expression of lamin A/C correlates with poor histological differentiation and prognosis in primary gastric carcinoma”. In: *Journal of Experimental & Clinical Cancer Research* 28 (2009), pp. 1–12.
- [63] Callinice D Capo-chichi et al. “Loss of A-type lamin expression compromises nuclear envelope integrity in breast cancer”. In: *Chinese journal of cancer* 30.6 (2011), p. 415.
- [64] Giovanna Maresca et al. “LMNA knock-down affects differentiation and progression of human neuroblastoma cells”. In: (2012).
- [65] Kunnathur Murugesan Sakthivel and Poonam Sehgal. “A novel role of lamins from genetic disease to cancer biomarkers”. In: *Oncology reviews* 10.2 (2016).

- [66] Naomi D Willis et al. “Lamin A/C is a risk biomarker in colorectal cancer”. In: *PloS one* 3.8 (2008), e2988.
- [67] Hea-Jin Jung et al. “Nuclear lamins in the brain—new insights into function and regulation”. In: *Molecular neurobiology* 47 (2013), pp. 290–301.
- [68] Hea-Jin Jung et al. “Regulation of prelamin A but not lamin C by miR-9, a brain-specific microRNA”. In: *Proceedings of the National Academy of Sciences* 109.7 (2012), E423–E431.
- [69] Brian C Capell and Francis S Collins. “Human laminopathies: nuclei gone genetically awry”. In: *Nature reviews genetics* 7.12 (2006), pp. 940–952.
- [70] David A Parry et al. “Heterozygous lamin B1 and lamin B2 variants cause primary microcephaly and define a novel laminopathy”. In: *Genetics in Medicine* 23.2 (2021), pp. 408–414.